

The planar thermal Hall conductivity in the Kitaev magnet α -RuCl₃.

Peter Czajka¹, Tong Gao¹, Max Hirschberger², Paula Lampen-Kelley^{3,4}, Arnab Banerjee⁶, Nicholas Quirk¹, David G. Mandrus^{3,4}, Stephen E. Nagler⁵, and N. P. Ong^{1,§}

¹*Department of Physics, Princeton University, Princeton, NJ 08544, USA*

²*Dept. of Applied Physics, The University of Tokyo,
7-3-1 Hongo, Bunkyo-ku, Tokyo 113-8656, Japan*

³*Department of Materials Science and Engineering,
University of Tennessee, Knoxville, Tennessee 37996, USA*

⁴*Materials Science and Technology Division, and* ⁵*Neutron Scattering Division,
Oak Ridge National Laboratory, Oak Ridge, Tennessee 37831, USA*

⁶*Department of Physics and Astronomy, Purdue University, West Lafayette, IN 47907-2036*

(Dated: January 21, 2022)

We report detailed measurements of the Onsager-like planar thermal Hall conductivity κ_{xy} in α -RuCl₃, a spin-liquid candidate of topical interest. With the thermal current \mathbf{J}_Q and magnetic field $\mathbf{B} \parallel \mathbf{a}$ (zigzag axis), the observed κ_{xy}/T varies strongly with temperature T (1-10 K). The results are well-described by bosonic edge excitations which evolve to topological magnons at large B . Fits to κ_{xy}/T yield a Chern number ~ 1 and a band energy $\omega_1 \sim 1$ meV, in agreement with sharp modes seen in electron spin-resonance experiments. The bosonic character is incompatible with half-quantization of κ_{xy}/T .

In the field of quantum spin liquids [1–3], the honeycomb magnet α -RuCl₃ has attracted considerable interest because it is proximate to the Kitaev Hamiltonian \mathcal{H}_K [4–12]. In 2006, Kitaev [13] published the exact solution for the ground state of \mathcal{H}_K , and found that the excitations are Majoranas and vortices. The Majorana excitations lead to a thermal Hall conductivity κ_{xy} that is half-quantized.

The thermal Hall effect provides a powerful probe of spin excitations, for e.g. in the pyrochlore Tb₂Ti₂O₇ [14] and the kagome magnet Cu(1-3, bdc) [15]. In 2018, evidence for a half-quantized κ_{xy} in α -RuCl₃ in the narrow interval $3.7 < T < 5$ K was reported in Ref. [16]. Half-quantization of κ_{xy}/T was also observed [17] with $\mathbf{B} \parallel \mathbf{a}$ but in a narrow field interval distinct from that in Ref. [16]. Subsequently, the authors of Ref. [18] reported that the planar κ_{xy} was strongly T dependent showing no trace of half-quantized behavior. In this report, large oscillations of κ_{xx} were observed with maximal amplitude within the window $7 < H < 11.5$ T. A third group recently reported observing a robust half-quantization signal in the planar geometry [19]. The conflicting results reflect the weak signal and large hysteretic and magnetocaloric effects below 4 K.

Adopting measures to mitigate these distortions, we have obtained κ_{xy} over a broad interval of T (0.5 to 10 K). Our results point to a view of κ_{xy} categorically distinct from the half-quantized picture. We show that κ_{xy} originates from bosonic edge-mode excitations that become topological magnons at large B . Whereas fermionic edge modes have been investigated intensively in quantum Hall systems, our experiment is possibly the first demonstration of neutral bosonic edge modes in a magnetic insulator.

In the experiment, both the thermal current \mathbf{J}_Q and \mathbf{B} are applied $\parallel \hat{\mathbf{x}} \parallel \mathbf{a}$. During each run lasting 8-10 h, B is incremented in steps $\delta B = 0.2$ T from -13 to +13

T (and back to -13 T) while T is regulated within ± 1 mK of its set-point. We adopt a step-probe protocol in which measurements of the sensors T_A , T_B and T_C are delayed by 150 s after each step-change. The protocol rigorously excludes contamination by the large transients caused by magnetocaloric and eddy-current heating effects. Hysteretic artefacts are eliminated by combining field sweep-up and -down curves. The 3 readings determine the values of λ_{yx} and λ_{xx} at each B .

Figure 1 (a) shows the explicitly B -antisymmetric thermal Hall signal ΔT_H^{asym} (proportional to the thermal Hall resistivity λ_{yx}) measured at 7.5 K in an in-plane $\mathbf{B} \parallel \hat{\mathbf{x}}$ (inset). At each B , the thermal Hall signal is obtained by combining the two readings $T_B - T_C$ and $T_A - T_C$, and field-antisymmetrizing. In Panel (b), the color map provides an overview of how λ_{yx} varies over the B - T plane. The large- λ_{yx} region above 4 K (red area) tapers to a thin neck at 7.5 T as T decreases to 1 K. Below 2.5 K, λ_{yx} becomes slightly negative in the small region shown in blue. The evolution of the field profiles of λ_{yx} is shown in Fig. 1c. At 9.22 K, the profile features a broad peak that narrows dramatically as $T \rightarrow 3.65$ K. At high B (> 10 T), λ_{yx} is strongly suppressed to values below our resolution for $T < 4$ K.

From the matrix inversion $\kappa_{ij} = [\lambda^{-1}]_{ij}$, we derive the curves of κ_{xy}/T vs. B which display a peak in the field profile (Fig. 1d). In the regime $B > 10$ T and $T < 4$ K, the matrix inversion leads to large uncertainties (caused by multiplying a near-zero λ_{yx} by a factor of $\sim 10^3$). Over the interval $0.5 < T < 10$ K, κ_{xy}/T does not show evidence of half-quantization (dashed line). Instead, the pervasive feature is strongly T -dependent κ_{xy} .

Figure 2 shows how κ_{xy}/T varies with T with B fixed at between 5 and 10 T. At each value of B , κ_{xy}/T falls monotonically towards zero as T decreases below 10 K. We have found that the steep T dependence is in quantitative agreement with edge modes populated by bosons

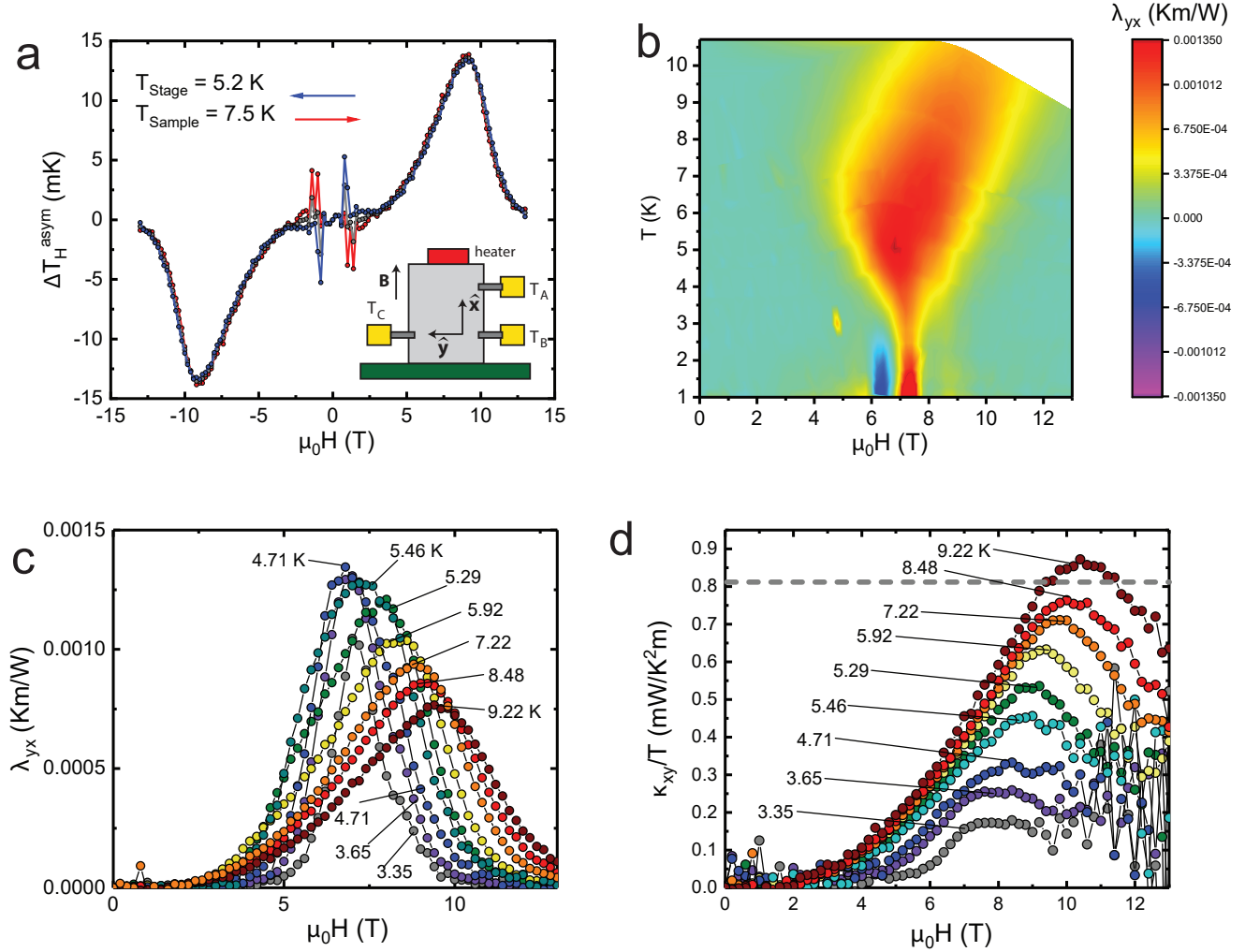


FIG. 1. Planar thermal Hall response of α -RuCl₃ in the interval $0.5 < T < 10.5$ K and field range $0 < B < 13$ T with $\mathbf{B} \parallel \mathbf{a}$. Panel (a) shows the B -antisymmetric thermal Hall signal ΔT_H^{asym} taken in sweep-up (red) and -down (blue) directions at 7.5 K (ΔT_H^{asym} is proportional to λ_{yx}). The inset shows the placements of thermometers measuring T_A , T_B and T_C . Panel (b): The color map constructed from ~ 50 traces of the thermal Hall resistivity λ_{yx} vs. B in the B - T plane (scale bar on right). The large- λ_{yx} region (in red) tapers down to a neck around 7.3 T, as $T \rightarrow 0.4$ K. Below 2.5 K, $\lambda_{yx} < 0$ in a sliver at 6.3 T (blue region). Panel (c) shows curves of λ_{yx} vs. B at fixed T . The peak in the field profiles narrows as $T \rightarrow 3.35$ K. Below 4 K, λ_{yx} is strongly suppressed to zero above 9.5 T. Panel (d) plots κ_{xy}/T vs. B (at fixed T) inferred from λ_{ij} . The non-intersecting curves imply that, at any fixed B , κ_{xy}/T is monotonic in T . Below 4.7 K the matrix inversion greatly amplifies the uncertainties in λ_{xy} for $B > 9$ T.

(solid curves).

First, a planar thermal Hall effect that is odd in \mathbf{B} is quite unexpected. In topological materials, however, the emergence of a Berry curvature $\mathbf{\Omega}$ that reverses sign with \mathbf{B} can lead to such a Hall response, as seen in ZrTe₅ [20]. For this purpose, we would need $\mathbf{\Omega} \parallel \hat{\mathbf{c}}^*$ (normal to the honeycomb layer) as well as to reverse sign with $\mathbf{B} \parallel \mathbf{a}$.

Recent calculations have shown that $\mathbf{\Omega}$ indeed emerges in α -RuCl₃ with high-intensity spots near each of the K points in the Brillouin zone (BZ) [21–23] (Fig. 3a, inset). At large B , the excitations, called topological magnons,

occupy bands in which the Chern number \mathcal{C}_n alternates in sign [21–23]. Significantly, when $\mathbf{B} \parallel \mathbf{a}$, $\mathbf{\Omega}$ reverses sign with \mathbf{B} [23, 28].

In a 2D magnet with finite $\mathbf{\Omega}$, the thermal Hall conductivity is given by [24, 25]

$$\frac{\kappa_{xy}}{T} = \frac{1}{\hbar V} \sum_{n, \mathbf{k}} \Omega_{n,z}(\mathbf{k}) \int_{\varepsilon_{n, \mathbf{k}}}^{\infty} d\varepsilon \frac{(\varepsilon - \mu)^2}{T^2} \left(-\frac{d\rho}{d\varepsilon} \right), \quad (1)$$

where the sum is over bands with dispersion $\varepsilon_{\mathbf{k}}$ and Berry curvature $\mathbf{\Omega}_n$, ρ is the distribution function of the relevant excitation, V is the sample volume, μ the chemical

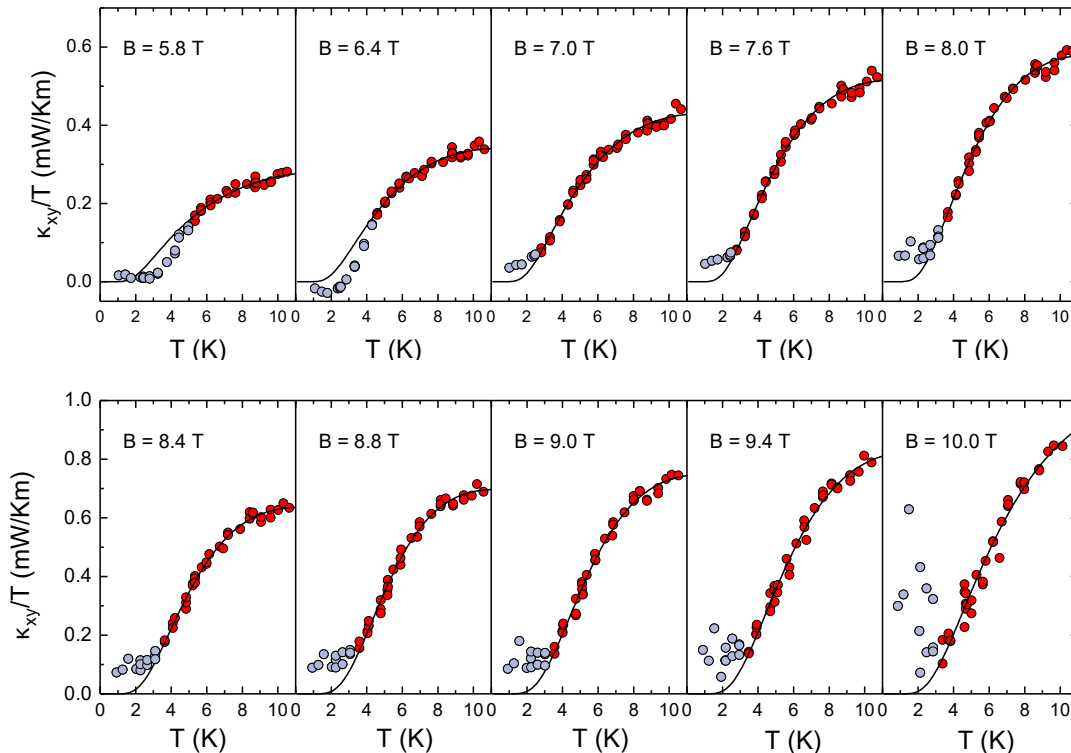


FIG. 2. Curves of κ_{xy}/T vs. T at B fixed at the ten values indicated. In each panel, the solid curves are fits to Eqs. 3 and 4. At each B , the fit yields the energies ω_1 and ω_2 and \mathcal{C}_{obs} . The grey circles represent weak deviations from the fits below 4 K. Just below the boundary of the zigzag phase ($B < 7$ T), excitations in the zigzag state lead to negative deviations (see also Fig. 3b). In the QSL state ($7 < B < 11$ T), positive deviations onset below 3 K and grow in amplitude as $T \rightarrow 0$. These seem to be related to the excitations that lead to oscillations in κ_{xx} (see Supplement).

potential and $\hbar = h/2\pi$ with h the Planck constant.

Semiclassically, we may regard a wave-packet subject to $\mathbf{\Omega}$ and the force $-\nabla U$ exerted by the wall potential U [25] (Fig. 3a, inset). The anomalous velocity $\mathbf{v}_A = -\nabla U \times \mathbf{\Omega}$ drives a circulating thermal current around the edges. A thermal gradient $-\nabla T \parallel \hat{\mathbf{x}}$ unbalances the excitation density between the warm edge $\parallel \hat{\mathbf{y}}$ and the cool edge, which leads to a net thermal current $\mathbf{J}_Q \parallel \hat{\mathbf{y}}$ (Fig. 3c). Crucially, the reversal of $\mathbf{\Omega}$ induced by reversing \mathbf{B} leads to an Onsager planar thermal Hall current.

If the excitations are fermions, Eq. 1 yields the (T -independent) Kane-Fisher result [26, 27]

$$\frac{\kappa_{xy}}{T} = \frac{\pi^2}{3} \frac{k_B^2}{h} \nu, \quad (\nu \in \mathbb{Z}). \quad (2)$$

where k_B is Boltzmann's constant.

By contrast, for bosons, Eq. 1 yields a very strong T dependence. In units of the universal thermal conductance k_B^2/h (and setting $\mu = 0$), Eq. 1 simplifies to

$$\frac{\mathcal{K}_H}{T} \equiv \frac{\kappa_{xy}/T}{k_B^2/h} = \sum_n \mathcal{C}_n c_2^{(n)}(\omega_n, T) \quad (3)$$

The function $c_2^{(n)}(\omega_n, T)$ is defined as [24, 25]

$$c_2^{(n)}(\omega_n, T) = \int_{u_{0n}}^{\infty} du u^2 (-d\rho/du), \quad (u_{0n} = \beta\omega_n(\mathbf{k})), \quad (4)$$

where $\rho = 1/(e^u - 1)$ and $\beta = 1/(k_B T)$. The lowest band is nearly flat [23]. Adopting the flat-band approximation, we used the winding-number equation $2\pi\mathcal{C}_n = \int_{\text{BZ}} d^2k \Omega_{n,z}(\mathbf{k})$ to relate $\Omega_{n,z}$ to \mathcal{C}_n .

At low T , we retain the 2 lowest bands in Eq. 3 (Fig. 3a and Supplement). Assuming that their Chern numbers alternate in sign ($\mathcal{C}_1 = -\mathcal{C}_2$), we have

$$\frac{\mathcal{K}_H}{T} = \mathcal{C}_1 \left[c_2^{(1)}(\omega_1, T) - c_2^{(2)}(\omega_2, T) \right]. \quad (5)$$

The overall scale of \mathcal{K}_H/T is fixed by \mathcal{C}_1 .

We find that Eq. 5 provides close fits to the observed κ_{xy}/T over a broad range of B (the fits were carried out on $\kappa_{xy}^{2D} = \kappa_{xy}d$ with $d = 5.72 \text{ \AA}$). In Fig. 2, the fits are shown as the solid curves. We have found that slight deviations from the fits (grey circles) reveal important information on the excitations.

For $B < 6.8$ T, κ_{xy}/T displays a weak, negative deviation (dip) below 3 K (in the blue region in Fig. 1b).

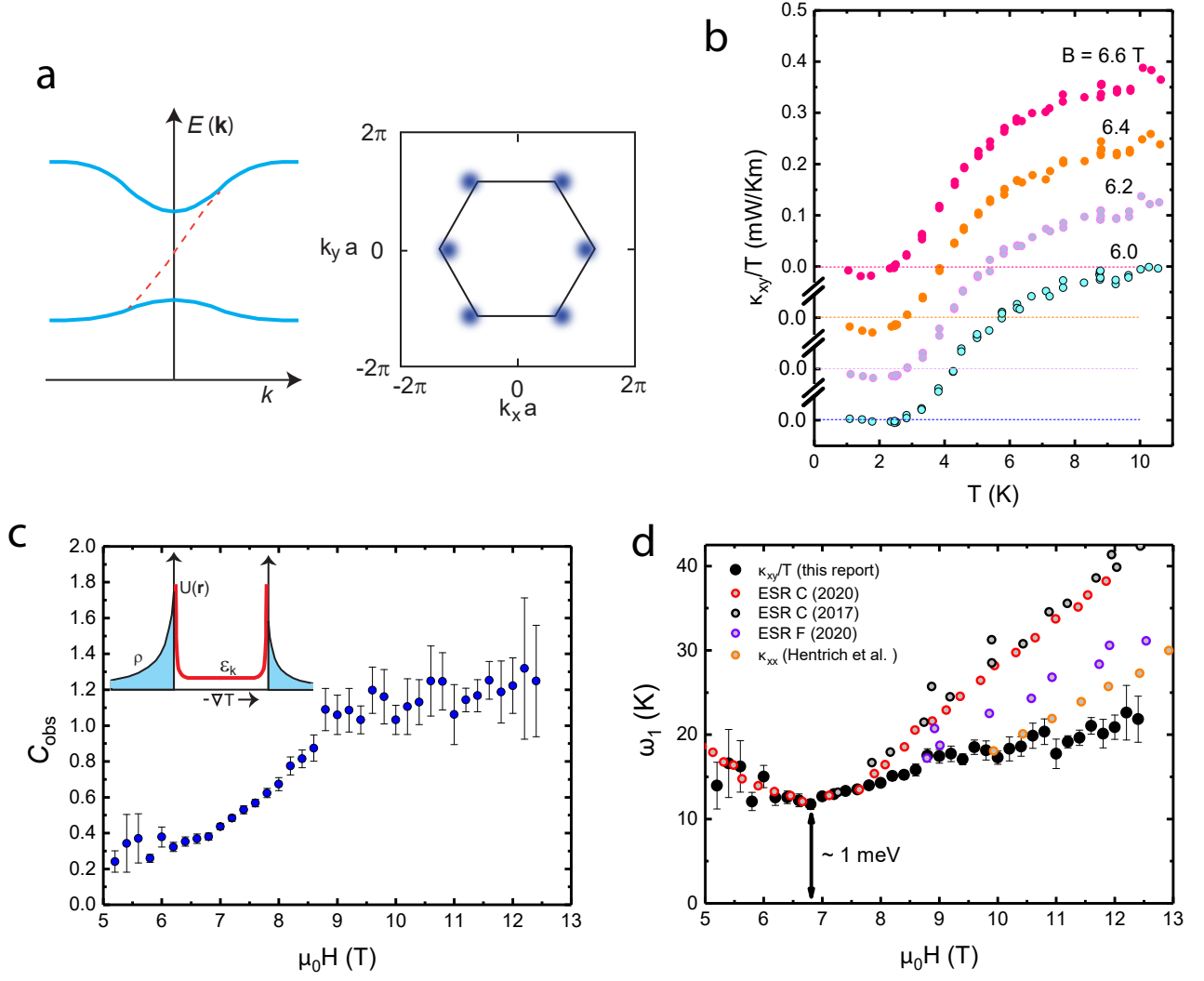


FIG. 3. Bosonic edge-mode and the planar κ_{xy} . Panel(a) shows a sketch of the two lowest magnon modes (blue curves) with $\omega_1 = 11.6$ K and $\omega_2 \simeq 50$ K. With $C = 1$ in the lowest band, an edge mode traverses the gap (dashed curve). The inset displays the high-intensity spots of the Berry curvature Ω calculated [23] for the lowest band with $\mathbf{B} \parallel \mathbf{a}$. Ω changes sign with \mathbf{B} . Panel (b): Curves of κ_{xy}/T vs. T with B fixed at 6.0, 6.2, 6.4 and 6.6 T (just inside the zigzag phase). Below 3 K, κ_{xy} displays a weak negative contribution. For clarity, we have shifted successive curves vertically by 0.1 mW/Km. Panel (c): The quantity C_{obs} defined in Eq. 6 derived from the fit at each B . As B increases, C_{obs} saturates to a value ~ 1.1 above 9 T, consistent with the Chern integer 1. In the inset, the profile of $U(\mathbf{r}) + \omega_1$ is sketched as the red curve. A gradient $-\nabla T \parallel \hat{\mathbf{x}}$ unbalances the excitation densities between the warm and cool edges to produce $\mathbf{J}_Q \parallel \hat{\mathbf{y}}$ (distribution ρ shaded in blue). Panel (d) shows the B dependence of the energy level ω_1 derived from the fit of κ_{xy}/T vs. T to Eq. 5 at each B . At the minimum (at 6.8 T), ω_1 agrees with the energy of the narrow mode seen in ESR (~ 1 meV). At large B , ω_1 is slightly lower than the ESR mode, and in better agreement with the energy extracted from κ_{xx} in Ref. [11].

The expanded view in Fig. 3b shows the dips in 4 traces of κ_{xy}/T vs. T . The negative dips imply that, once we enter the ordered phase (below 7 T), the spin excitation branches deviate from Eq. 3. The weak negative dip feature also appears in calculations of κ_{xy} (see Figs. 3 and 6 in Ref. [28]). Weak, positive deviations are also observed below ~ 10 T. These deviations represent the growth of excitations in the QSL state as $T \rightarrow 0$. Within the uncertainties, they scale with the amplitude of the

oscillations in κ_{xx} (Supplement).

Away from these deviations, the fits shown in Fig. 2 describe quite accurately the strong T dependence of κ_{xy}/T over a broad range of B . At each B , the fit yields the 2 energies ω_1 and ω_2 (in Eq. 4) as well as the dimensionless quantity C_{obs} discussed next.

Dividing Eq. 5 across by the T -dependent factor

$[c_2^{(1)}(\omega_1, T) - c_2^{(2)}(\omega_2, T)]$, we define

$$C_{\text{obs}} \equiv (\mathcal{K}_H/T)/[c_2^{(1)}(\omega_1, T) - c_2^{(2)}(\omega_2, T)], \quad (6)$$

which can be compared with C_1 . C_{obs} is plotted vs. B in Fig. 3c.

We find that C_{obs} starts off small (~ 0.3 at 5 T) but increases to attain a plateau above 9 T. Within the experimental uncertainty, the nearest integer at the plateau is $C_{\text{obs}} \simeq 1$. The strong T dependence of κ_{xy}/T largely arises from the bosonic distribution in the integrand of $c_2^{(n)}$ (Eq. 4). Remarkably, once this is factored out, the overall amplitude in the polarized state at high fields is fixed by the integer $C_{\text{obs}} \simeq 1$.

We show next that the energy ω_1 derived from the fits of κ_{xy}/T to Eq. 1 closely agrees with the energy of the dominant sharp mode seen in electron spin resonance (ESR) [29, 30], microwave absorption [8, 31] and neutron-scattering experiments [33]. The energy of the second band is found to be $\omega_2 \sim 50 \pm 10$ K with a large uncertainty. In the field interval above B_c (from 7.3 to 14 T), α -RuCl₃ displays a rich magnetic resonance spectrum with 4 sharp modes (C , D , E and F) [29] superposed on a broad continuum suggestive of excitations [8, 31]. The broad continuum was observed also in microwave absorption and inelastic neutron scattering experiments [33]. At $B=7.3$, the two lowest modes C and F are degenerate at 0.27 THz (1.1 meV). As B is raised to 16 T, both increase steeply to 1.1 THz (for C) and 0.9 THz (F). These modes are also seen in exact diagonalization of a 24-spin model [32]. Close to B_c , ω_1 inferred from κ_{xy}/T agrees remarkably well with the degenerate values of C and F . At large B , ω_1 is lower than C (C arises from vertical $\Delta\mathbf{q} = 0$ transitions [30] at the zone center Γ). This

suggests that, as C rises steeply with B , κ_{xy} is weighted towards lower-lying excitations from elsewhere in the BZ. The curve of $\omega_1(B)$ agrees with the energy scale inferred in Ref. [11] from $\kappa_{xx}(T)$.

As discussed in Refs. [29, 30, 32], the sharp ESR mode C is increasingly dominant at large B but the broad background excitation continuum persists. From this viewpoint, the observed saturation of C_{obs} to 1 above 9 T in Fig. 3d is physically appealing. As the dominant excitations become increasingly magnon-like, the topological Hall current, expressed as C_{obs} , approaches 1. For $B < 7$ T (zig-zag state) the vanishing of κ_{xy} (aside from the negative dip near 6.3 T) suggests that Ω is very small.

The physical picture that emerges is that the planar κ_{xy} derives from spin excitations that live at the relatively high energy scale $\omega_1 \sim 1$ meV (11.6 K). A large Berry curvature drives these excitations as an edge-mode thermal current, which results in an Onsager-type thermal Hall current whose magnitude corresponds to a Chern number of 1 at fields above 9 T. At all B , the bosonic character leads to strong suppression of κ_{xy} to near zero below 3 K. Because this strong T dependence precludes a fermionic description, a critical review of reports of a half-quantized κ_{xy}/T in α -RuCl₃ seems warranted. Finally, we note that ω_1 is not a bulk “spin gap”. The sharp modes coexist with a broad continuum corresponding to spin excitations that extend well below ω_1 . We emphasize that the magnons are only well-defined above ~ 10 T [33]. As we lower B into the spin-liquid state, the excitations are increasingly less magnon-like, as seen in the deviations from the fit to Eq. 3 as well as the steep decrease of C_{obs} (Fig. 3c). The deviations provide clues to the excitations in the spin-liquid state. In the low- T limit, the edge-mode engendered κ_{xy} vanishes altogether while novel bulk features emerge to define the oscillations observed in κ_{xx} [18, 34].

-
- [1] Savary, L. & Balents, L., Quantum spin liquids: a review, *Rep. Prog. Phys.* **80**, 106502 (2017). doi:10.1088/0034-4885/80/1/016502
- [2] Zhou, Y., Kanoda, K. & Ng, T.K. Quantum spin liquid states, *Rev. Mod. Phys.* **89**, 025003 (2017). DOI: 10.1103/RevModPhys.89.025003
- [3] Hidenori Takagi, Tomohiro Takayama, George Jackeli, Giniyat Khaliullin and Stephen E. Nagler, Concept and realization of Kitaev quantum spin liquids, *Nat. Rev. Phys.* **1**, 264-280 (2019). doi.org/10.1038/s42254-019-0038-2
- [4] Jackeli, G. & Khaliullin, G., Mott Insulators in the Strong Spin-Orbit Coupling Limit: From Heisenberg to a Quantum Compass and Kitaev Models, *Phys. Rev. Lett.* **102**, 017205 (2009).
- [5] Plumb, K. W. *et al.*, α -RuCl₃: a spin-orbit assisted Mott Insulator on a honeycomb lattice. *Phys. Rev. B* **90**, 041112 (2014).
- [6] Banerjee, A. *et al.*, Proximate Kitaev quantum spin liquid behavior in a honeycomb magnet. *Nat. Mater.* **15**, 733-740 (2016).
- [7] Sears, J. A. *et al.*, Phase diagram of α -RuCl₃ in an in-plane magnetic field. *Phys. Rev. B* **95**, 180411 (2017).
- [8] Z. Wang, S. Reschke, D. Huvonen, S.H. Do, K. Y. Choi, M. Gensch, U. Nagel, T. Room, and A. Loidl, Magnetic excitations and continuum of a possibly field-induced quantum spin liquid in α -RuCl₃, *Phys. Rev. Lett.* **119**, 227202 (2017). DOI: 10.1103/PhysRevLett.119.227202
- [9] Leahy, I. A. *et al.*, Anomalous thermal conductivity and magnetic torque response in the honeycomb magnet α -RuCl₃, *Phys. Rev. Lett.* **118**, 187203 (2017).
- [10] Banerjee, A. *et al.*, Excitations in the field-induced quantum spin liquid state of α -RuCl₃. *npj Quantum Materials* (2018) 3:8 ; doi:10.1038/s41535-018-0079-2
- [11] Hentrich, R. *et al.*, Unusual phonon heat transport in α -RuCl₃: Strong spin-phonon scattering and field-induced spin gap. *Phys. Rev. Lett.* **120**, 117204 (2018).
- [12] Lampen-Kelley, P. *et al.*, Anisotropic susceptibilities in the honeycomb Kitaev system α -RuCl₃. *Phys. Rev. B* **98**, 100403 (2018).

- [13] Kitaev, A., Anyons in an exactly solved model and beyond, *Ann. Phys.* **321**, 2-111 (2006).
- [14] Max Hirschberger, Jason W. Krizan, R. J. Cava, N. P. Ong, Large thermal Hall conductivity of neutral spin excitations in a frustrated quantum magnet, *Science* **348**, 106 (2015). DOI: 10.1126/science.1257340
- [15] Max Hirschberger, Robin Chisnell, Young S. Lee, and N. P. Ong, Thermal Hall Effect of Spin Excitations in a Kagome Magnet, *Phys. Rev. Lett.* **115**, 106603 (2015). DOI: 10.1103/PhysRevLett.115.106603
- [16] Kasahara, Y. *et al.*, Majorana quantization and half-integer thermal quantum hall effect in a Kitaev spin liquid. *Nature* **559**, 227-231 (2018).
- [17] T. Yokoi, S. Ma, Y. Kasahara, S. Kasahara, T. Shibauchi, N. Kurita, H. Tanaka, J. Nasu, Y. Motome, C. Hickey, S. Trebst and Y. Matsuda, Half-integer quantized anomalous thermal Hall effect in the Kitaev candidate α -RuCl₃, *Science* **373**, 568-572 (2021). DOI: 10.1126/science.aay5551
- [18] Czajka, P. *et al.*, Oscillations of the thermal conductivity in the spin-liquid state of α -RuCl₃, *Nature Physics* **17**, 915-919 (2021). doi.org/10.1038/s41567-021-01243-x
- [19] J. A. N. Bruin, R. R. Claus, Y. Matsumoto, N. Kurita, H. Tanaka and H. Takagi, Robustness of the thermal Hall effect close to half-quantization in a field-induced spin liquid state, *cond-mat arXiv:2104.12184*.
- [20] Liang, T. *et al.*, Anomalous Hall effect in ZrTe₅, *Nat. Phys.* **14**, 451-455 (2018). doi.org/10.1038/s41567-018-0078-z
- [21] McClarty, P. A. and Dong, X.-Y. and Gohlke, M. and Rau, J. G. and Pollmann, F. and Moessner, R. and Penc, K., Topological magnons in Kitaev magnets at high fields, *Phys. Rev. B* **98**, 060404 (2018). DOI: 10.1103/PhysRevB.98.060404
- [22] Joshi, Darshan G., Topological excitations in the ferromagnetic Kitaev-Heisenberg model, *Phys. Rev. B* **98**, 060405 (2018). DOI: 10.1103/PhysRevB.98.060405
- [23] Chern, Li Ern and Zhang, Emily Z. and Kim, Yong Baek, Sign Structure of Thermal Hall Conductivity and Topological Magnons for In-Plane Field Polarized Kitaev Magnets, *Phys. Rev. Lett.* **126**, 147201 (2021). DOI: 10.1103/PhysRevLett.126.147201
- [24] Ryo Matsumoto and Shuichi Murakami, Theoretical Prediction of a Rotating MagnonWave Packet in Ferromagnets, *Phys. Rev. Lett.* **106**, 197202 (2011) DOI: 10.1103/PhysRevLett.106.197202
- [25] Ryo Matsumoto and Shuichi Murakami, Rotational motion of magnons and the thermal Hall effect, *Phys. Rev. B* **84**, 184406 (2011). DOI: 10.1103/PhysRevB.84.184406
- [26] C. L. Kane and Matthew P.A. Fisher, Quantized thermal transport in the fractional quantum Hall effect, *Phys. Rev. B* **55**, 15 832 (1997).
- [27] Yanting Teng, Yunchao Zhang, Rhine Samajdar, Mathias S. Scheurer, and Subir Sachdev, Unquantized thermal Hall effect in quantum spin liquids with spinon Fermi surfaces, *Phys. Rev. Res.* **2**, 033283 (2020). DOI: 10.1103/PhysRevResearch.2.033283
- [28] Zhang, Emily Z. and Chern, Li Ern and Kim, Yong Baek, Topological magnons for thermal Hall transport in frustrated magnets with bond-dependent interactions, *Phys. Rev. B* **103**, 174402 (2021). DOI: 10.1103/PhysRevB.103.174402
- [29] A. N. Ponomaryov, E. Schulze, J. Wosnitzer, P. Lampen-Kelley, A. Banerjee, J.-Q. Yan, C. A. Bridges, D. G. Mandrus, S. E. Nagler, A. K. Kolezhuk, and S. A. Zvyagin, Unconventional spin dynamics in the honeycomb-lattice material α -RuCl₃: High-field electron spin resonance studies, *Phys. Rev. B* **96**, 241107(R) (2017). DOI: 10.1103/PhysRevB.96.241107
- [30] A. N. Ponomaryov, L. Zviagina, J. Wosnitzer, P. Lampen-Kelley, A. Banerjee, J.-Q. Yan, C. A. Bridges, D. G. Mandrus, S. E. Nagler, and S. A. Zvyagin, Nature of Magnetic Excitations in the High-Field Phase of α -RuCl₃. *Phys. Rev. Lett.* **125**, 037202 (2020). DOI: 10.1103/PhysRevLett.125.037202
- [31] C. Wellm, J. Zeisner, A. Alfonsov, A. U. B. Wolter, M. Roslova, A. Isaeva, T. Doert, M. Vojta, B. Buchner and V. Kataev, Signatures of low-energy fractionalized excitations in α -RuCl₃ from field-dependent microwave absorption, *Phys. Rev. B* **98**, 184408 (2018). DOI: 10.1103/PhysRevB.98.184408
- [32] Stephen M. Winter, Kira Riedl, David Kaib, Radu Coldea, and Roser Valenti, Probing α -RuCl₃ Beyond Magnetic Order: Effects of Temperature and Magnetic Field, *Phys. Rev. Lett.* **120**, 077203 (2018). DOI: 10.1103/PhysRevLett.120.077203
- [33] Balz, C. *et al.*, Finite field regime for a quantum spin liquid in α -RuCl₃. *Phys. Rev. B* **100**, 060405(R) (2019).
- [34] Inti Sodemann Villadiego, Pseudoscalar U(1) spin liquids in α -RuCl₃, *Phys. Rev. B* **104**, 195149 (2021). DOI: 10.1103/PhysRevB.104.195149

* * *

[§]Corresponding author email: npo@princeton.edu

[†] Present address of MH:

Acknowledgements

We acknowledge useful discussions with Patrick Lee and Inti Sodemann. The research was supported by the U.S. Department of Energy (award DE-SC0017863). NPO was supported by the Gordon and Betty Moore Foundation's EPiQS initiative through grant GBMF4539.

Author contributions

PC performed the measurements and analysed the data together with NPO, who proposed the experiment. MH developed many of the experimental techniques and pro-

vided guidance on interpreting the results. NQ measured the crystal dimensions. AB, PLK, and SEN provided guidance on prior results. The sample was grown at Oak Ridge National Laboratory by PLK, JY and DGM. The manuscript was written by PC and NPO with input from all authors.

Additional Information

Supplementary information is available in the online version of the paper. Correspondence and requests for materials should be addressed to NPO.

Competing financial interests

The authors declare no competing financial interests.